Retrieval Algorithm for the Column CO_2 Mixing Ratio from Pulsed Multi-Wavelength Lidar Measurements

Xiaoli Sun[1], James B. Abshire[1,2], Anand Ramanathan,[1,3], Stephan R. Kawa[1], and Jianping Mao[1,2]

[1]NASA Goddard Space Flight Center, Science and Exploration Directorate, Greenbelt, Maryland, USA
5 [2]University of Maryland, CRESST II, College Park, Maryland, USA
[3]Audible, Inc., Newark, New Jersey, USA

Correspondence to: Xiaoli Sun (xiaoli.sun-1@nasa.gov)

Abstract. The retrieval algorithm for CO_2 column mixing ratio from measurements of a pulsed multi-wavelength, integrated path differential absorption (IPDA) lidar is described. The lidar samples the shape of the 1572.33 nm CO_2 absorption line at multiple wavelengths. The algorithm uses a least-squares fit between the CO_2 line shape computed from a layered atmosphere model and that sampled by the lidar. In addition to the column average CO_2 dry air mole fraction (XCO_2), several other parameters are also solved simultaneously from the fit. These include the Doppler shift at the received laser signal wavelength, the product of the surface reflectivity and atmospheric transmission, and a linear trend in the lidar receiver's spectral response. The algorithm can also be used to solve for the average water vapor mixing ratio, which produces a secondary absorption in the wings of the CO_2 absorption line under humid conditions. The least-squares fit is linearized about the expected XCO_2 value which allows the use of a standard linear least-squares fitting method and software tools. The standard deviation of the retrieved XCO_2 is obtained from the covariance matrix of the fit. The averaging kernel is also provided similarly to that used for passive trace-gas column measurements. Examples are presented of using the algorithm to retrieve XCO_2 from measurements of the NASA Goddard airborne CO_2 Sounder lidar that were made at constant altitude and during spiral-down profile maneuvers.

1 Introduction

Accurate remote sensing of atmospheric CO_2 from Earth orbiting satellites is a key component in a long-term carbon-climate observing system (Sellers et al., 2018). Airborne and spaceborne lidar can be used to remotely monitor the global CO_2 and other trace-gas concentrations under conditions that are inaccessible to passive space-borne CO_2 measurement missions, such as GOSAT (Kuze et al., 2016), OCO-2 (Crisp, 2017), and OCO-3 (Eldering et al., 2017; 2019). Studies have shown (Kawa et al., 2018) that a polar orbiting integrated path differential absorption (IPDA) lidar can measure XCO_2 with low bias and high precision at all sun angles, seasons and latitudes using a constant nadir-zenith illumination and observation geometry. A pulsed IPDA lidar also provides the range-resolved atmospheric backscatter profiles, so that return signals from the surface, clouds, and aerosols can be uniquely separated (Allan et al., 2019). This allows pulsed IPDA lidar to measure XCO_2 to the surface, cloud tops, or both (Ramanathan et al., 2015). Because the laser pulses reflected from clouds, aerosols and surface are separated in time, the XCO_2 retrievals to the ground surface are not biased by scattering from clouds and aerosols (Mao et al., 2018).

Several types of dual wavelength (on-line and off-line) IPDA lidar have been demonstrated previously for measuring XCO_2 from aircraft (Spiers et al., 2011; Menzies et al., 2014; Jacob et al., 2019; Dobler et al., 2013; Campbell et al., 2020; Refaat et al., 2016, 2020, 2021; and Amediek et al., 2017). A multi-wavelength IPDA lidar has also been reported (Zhu et al., 2019, 2020). The retrieval algorithms used in these IPDA lidar calculate the ratios of on-line to the off-line atmosphere transmission, convert them to differential absorption optical depths (DAOD), and then solve for XCO_2 from the DAOD based on atmospheric transmission models. For the multi-wavelength lidar, a series of DAODs are calculated and a least-squares fit is used to solve for XCO_2 (Han et al., 2020). The XCO_2 can be solved directly from the DAOD, however, these algorithms rely on the accurate knowledge of the line shape of the CO_2 absorption. They are sensitive to measurement biases due uncertainties in spectroscopy and meteorological conditions that affect the line shape. They also require precise knowledge of the laser wavelengths, the lidar receiver optical transmission versus wavelength, and the Doppler shift of the received laser signals.

NASA Goddard Space Flight Center (GSFC) has developed an airborne multi-wavelength CO_2 Sounder lidar and demonstrated XCO_2 measurements through a series of airborne campaigns (Abshire et al., 2010, 2013, 2014, 2018; Ramanathan et al., 2013, 2015, 2018; Mao et al., 2018). Its retrieval compares the lidar-sampled line shape with one computed from an atmosphere model to retrieve XCO_2. Several other parameters, such as the Doppler shift, surface reflectance, and the lidar receiver spectral are solved simultaneously via a least-squares fit. The retrieval algorithm is similar to those used for passive trace gas measurements with modifications specifically for the lidar measurement. Although this multiwavelength approach requires more laser power to achieve a given XCO_2 measurement precision, it provides more tolerance to the uncertainties in the CO_2 absorption line shape, lidar receiver response, and Doppler shift, so that the retrieved XCO_2 is more robust against bias errors.

This paper describes the retrieval algorithm for the multi-wavelength CO_2 Sounder lidar and provides a framework for similar IPDA lidar for other atmospheric gas measurements. Parts of the algorithm have been reported earlier (Ramanathan et al., 2013, 2015, 2018). This paper gives a complete description of the algorithm, the mathematical derivations, signal processing techniques, estimation error, and averaging kernel. An example of using of the algorithm to analyze measurements from the airborne CO_2 Sounder lidar is also presented.

2. Measurement Approach

The measurement geometry for the CO_2 Sounder lidar is shown in Fig. 1. The lidar transmits laser pulses toward nadir and its receiver telescope collects the optical signal backscattered from the atmosphere and the surface. Figure 2 shows a block diagram of the airborne CO_2 Sounder lidar, which was developed as an airborne demonstrator for NASA's Active Sensing of CO_2 Emissions over Nights, Days, & Seasons (ASCENDS) mission (Kawa et al., 2018). The laser consists of a tunable seed laser, a pulsed modulator and a power amplifier. The seed laser module consists of two single-frequency continuous wave (CW) diode lasers. One is the reference laser whose wavelength locked to the center of the CO_2 absorption line in a gas cell.

The other diode laser is tunable and its wavelength is locked to that of the master, plus a programmable offset frequency. The offset frequency is step-tuned across the CO_2 absorption line. The number of laser wavelengths in the scan and the exact wavelength of each laser pulse are digitally pre-programmed and can be adjusted via software commands (Numata et al., 2012). An electro-optical modulator is used to gate the output of the slave laser into 1-μsec wide pulses. The laser pulses are then amplified by a multi-stage commercial fiber laser amplifier. The airborne lidar's laser pulse rate is 10 KHz and there are 30 wavelengths per scan, which gives a wavelength scan rate of about 300 Hz. The transmitted laser pulse energy at each wavelength is also sampled and the results are used to normalize the received signal to correct for fluctuations in the transmitted laser energy with wavelength.

The lidar receiver detects and records the received laser pulse waveform over the entire atmosphere column travelled by the laser pulses. In the airborne lidar all signals are digitized and recorded and the lidar analysis is performed on ground after the flight. The received signals from the scattering surface are used to retrieve XCO_2. The signals before the ground returns are used to obtain the atmosphere backscatter profiles as an ancillary data set. The signals recorded after the ground returns are used to estimate the solar background, the detector dark noise, and the baseline voltage offset in the detector output. The baseline offset is subtracted from the signal before calculating the ground return pulse energies. The times-of-flight of the laser pulse to the targeted scattering surface are used to determine the atmosphere column height over which the CO_2 is measured.
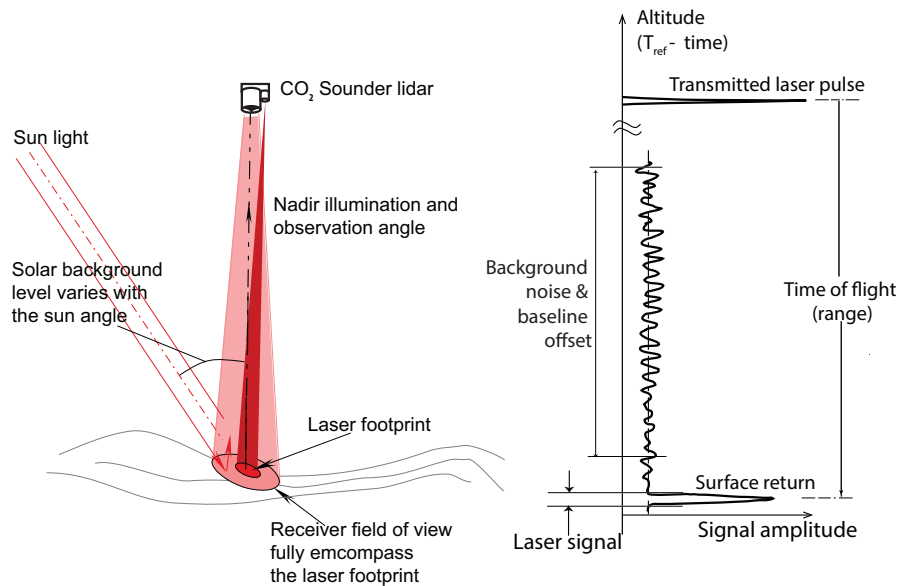
Figure 1. Illustrations of the CO_2 Sounder lidar measurement geometry and received signal at a single laser wavelength.
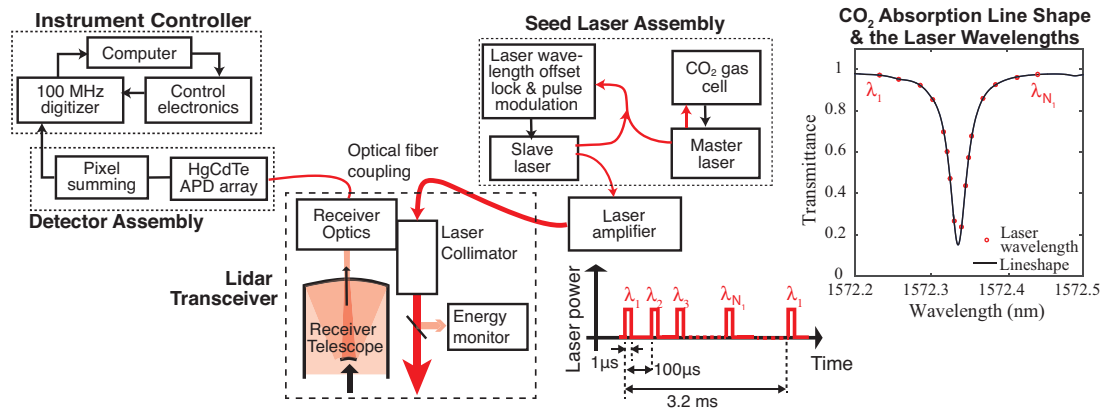
Figure 2. Block diagram of the airborne CO$_2$ Sounder lidar.

3. Lidar Signal Processing and Atmosphere Modelling

An overview of the retrieval algorithm for lidar data is shown in Fig. 3. The initial processing consists of (a) processing the stored lidar data to estimate ranges to the reflecting surfaces and form a series of atmosphere transmission measurements across the CO$_2$ absorption line; (b) generating a CO$_2$ absorption line shape from the radiative transfer model and meteorological data at the time and location of lidar measurements; and (c) performing a least-squares fit of the modelled line shape function to the measurements to solve for XCO$_2$ and other parameters.

3.1. Lidar Signal Processing

The signal waveforms are first corrected for the detector baseline offset and other instrument characteristics and then scaled to the received optical signal power. The pulse energies from the scattering surfaces are calculated by integrating the received pulse waveforms over the pulse width interval. The relative atmosphere transmittances for all laser wavelengths are calculated by dividing the received pulse energies by the transmitted ones and then multiplying by the square of the range from the lidar to the reflecting surface. The signal to noise ratio (SNR) of the atmospheric transmittances at each wavelength is estimated based on the received signal energy, the estimated background noise, and the detector noise. Finally, a least-squares fit of the modelled line shape to the lidar measurements is used to estimate XCO$_2$ along with the other parameters.

The lidar returns from clouds are identified by comparing the elevations of the lidar returns, namely, aircraft altitude minus the lidar range, to the surface elevation from either the on-board radar measurements or from a Digital Elevation Model (DEM). For dense clouds, the laser energies reflected from the cloud tops are usually sufficient for XCO$_2$ retrievals (Mao et al., 2018). For thin clouds and aerosols, the laser pulses can often reach the ground surface and be received at the lidar with sufficient energy to allow useful XCO$_2$ retrievals. The signal waveform before ground return can be averaged to obtain the atmospheric backscatter profiles at the laser wavelength, which gives information about the heights and densities of thin clouds and aerosols (Allan et al., 2019).
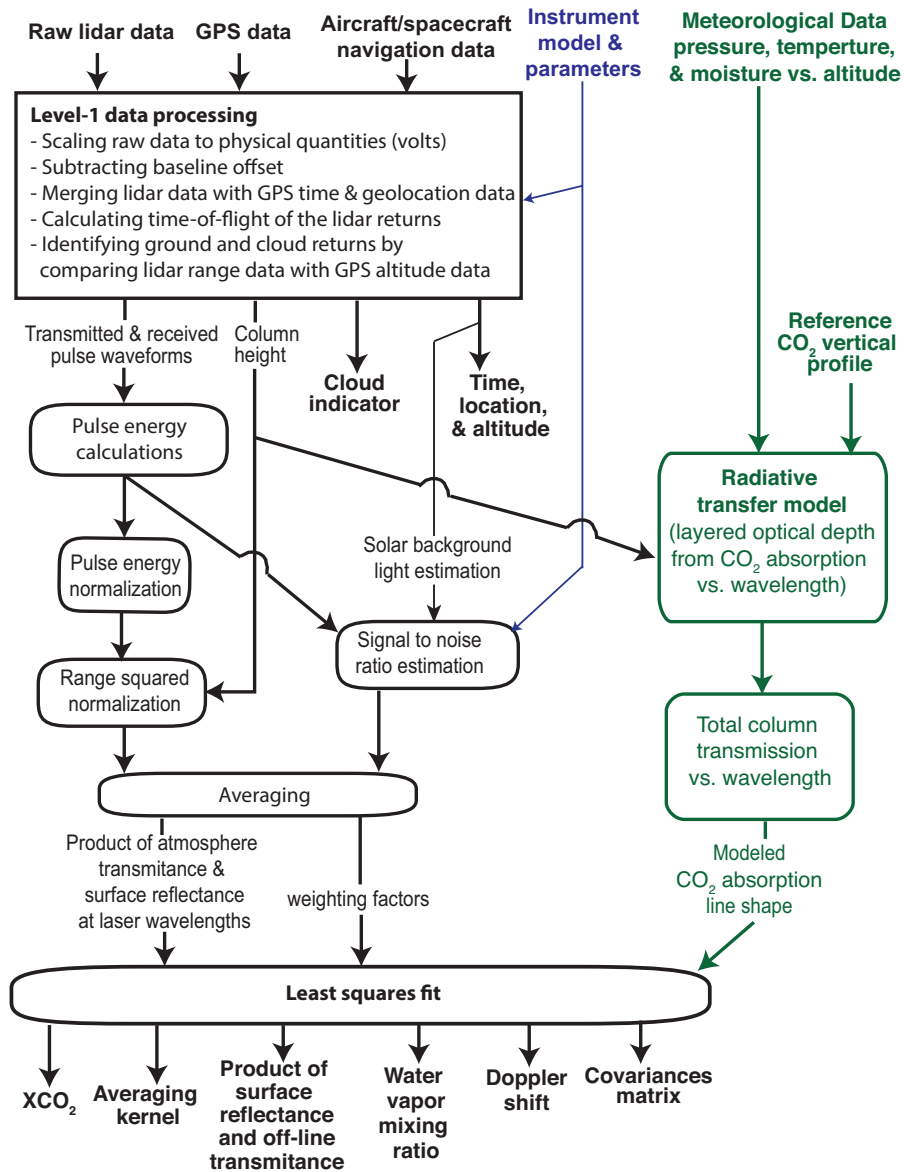
Figure 3. Flowchart of the XCO_2 retrieval algorithm for the CO_2 Sounder lidar.

3.2. Model for the Lidar Signals

The average signal pulse energy reflected from the scattering surface can be calculated from the lidar equation (McManamon, 2019), as

$$E_r(\lambda) = E_t(\lambda) \cdot T_A^2(\lambda) \frac{r_s}{\pi} \cdot \frac{A_r}{R^2} \cdot \eta_r \tag{1}$$

where

115          $E_r(\lambda)$ and $E_t(\lambda)$ are the received and transmitted laser pulse energies at laser wavelength λ;

         $T_A(\lambda)$ is the one-way atmosphere transmission at laser wavelength λ;

         r_s is the diffuse surface reflectance in nadir direction;

         A_r is the light collecting area of the receiver telescope;

         R is the range from the lidar to the scattering surface (the column height);

120   η_r is the receiver optical transmission efficiency.

The product of the surface reflectance and the two-way atmospheric transmission can be calculated from the received laser pulse energy after correcting for the range, as

$$y(\lambda) = r_s T_A^2(\lambda) = \left(\frac{\pi}{A_r \eta_r}\right)\left[\frac{E_r(\lambda)}{E_t(\lambda)} \cdot \frac{1}{R^2}\right]. \tag{2}$$

125 The term in the parenthesis of the right-hand side of Eq. (2) is a constant related to the lidar receiver. The telescope diameter and overall optical transmission are measured in the lab. The optical transmission can also be calibrated in flight by flying over an area where the surface reflectance and the atmospheric transmission are known from independent measurements. The term in brackets consists of variables measured by the lidar.

3.3. Model for the CO_2 Absorption Line Shape

130 The total atmospheric transmission from the lidar to the surface can be written as

$$T_A^2(\lambda) = T_{CO2}^2(\lambda) \cdot T_w^2(\lambda) \cdot T_o^2. \tag{3}$$

Here , $T_{CO2}^2(\lambda)$ and $T_w^2(\lambda)$ are the two-way atmospheric transmissions of CO_2 and water vapor at laser wavelength λ. The term T_o^2, accounts for the transmission of aerosols and other particles, which are independent of the laser wavelength. T_o^2 is often called the off-line atmospheric transmission. Note that Eq. (3) and the XCO_2 measurement is for the atmosphere column from

135 the lidar to the surface. This is different from the passive remote sensing measurement where the incident light from the sun and the reflected light are at an angle and go through different atmosphere columns.

       To compute the transmission line shapes of CO_2 and water vapor, the atmosphere is divided into a number of layers. The total transmission is modelled as the product of the individual transmissions of all the layers travelled by the laser pulse. The layered transmission is calculated from the layered radiative transfer atmospheric model, which takes into account the

140 effects of the temperature, pressure, and humidity for each layer. The vertical profiles of temperature, pressure and humidity are obtained from a meteorological analysis model, or, when possible, from in situ atmospheric measurements made during aircraft spiral-down maneuvers.

       The atmospheric transmissions of each layer for each of the lidar wavelength across the CO_2 absorption line are calculated by using the Beer-Lambert law. The total two-way transmission due to CO_2 can be written as

145 $$T_{CO2}^2(\lambda_i) = exp\left[-2\sum_{j=1}^{N_2}\rho_{CO2}(H_j)\sigma_{CO2}(H_j,\lambda_i)\Delta H_j\right] \tag{4}$$

where

$i = 1,2,\ldots,N_1$ is the index for the laser wavelengths with N_1 the total number of laser wavelengths used in the lidar measurements;

$j = 1,2,\ldots,N_2$ is the index for the atmosphere layer with N_2 the total number atmospheric layers;

150 $\rho_{CO2}(H_j)$ is the molecular density of CO_2 for the jth layer;

H_j is the average altitude of the jth layer;

$\sigma_{CO2}(H_j,\lambda_i)$ is the absorption cross-section of a CO_2 molecule in the jth layer at the ith wavelength.

Here we assumed that the laser wavelengths are known precisely and the laser spectral line width is much narrower than the CO_2 absorption line width. For the CO_2 Sounder lidar, the laser is step locked to an on-board CO_2 gas cell with fixed

155 frequency offsets in each scan. The frequency accuracy is <1 MHz peak to peak and the linewidth is about 30 MHz (Numata et al., 2012), which are small compared to the CO_2 absorption linewidth. It has been shown that for lidar measurements of XCO_2 such small laser frequency deviations are negligible compared to other noise sources (Chen et al., 2012, 2014, 2015, 2019).

The modelled optical transmission due to CO_2 can also be expressed in terms of the optical depth (OD) defined as the

160 absolute value of the logarithm of the one-way atmospheric transmission, as

$$T_{CO2}^2(\lambda_i) = exp[-2OD_{CO2}(\lambda_i)] \tag{5}$$

and

$$OD_{CO2}(\lambda_i) = \sum_{j=1}^{N_2}\rho_{CO2}(H_j)\sigma_{CO2}(H_j,\lambda_i)\Delta H_j = \sum_{j=1}^{N_2}\Delta OD_{CO2}(H_j,\lambda_i) \tag{6}$$

where $OD_{CO2}(\lambda_i)$ is the column OD at wavelength λ_i and $\Delta OD_{CO2}(H_j,\lambda_i) = \sum_{j=1}^{N_2}\rho_{CO2}(H_j)\sigma_{CO2}(H_j,\lambda_i)\Delta H_j$ is the OD of the

165 atmosphere layer due to CO_2 absorption at wavelength λ_i and altitude H_j.

The molecular density of CO_2 for the jth layer can be expressed as

$$\rho_{CO2}(H_j) = xco2(H_j)\,\rho_{air}(H_j), \tag{7}$$

where $xco2(H_j)$ is the CO_2 mixing ratio and $\rho_{air}(H_j)$ is the dry air molecular density at altitude H_j.

In our XCO_2 retrieval algorithm the layered OD is calculated by using the HITRAN 2008 spectroscopy database

170 (Rothman et al., 2009) and the Line-By-Line Radiative Transfer Model (LBLRTM) V12.1, (Clough et al., 1992; Clough and Iacono, 1995), for a given CO_2 mixing ratio and meteorological vertical profiles at the time and location of the lidar measurement.

The atmospheric pressure, temperature and water vapor can cause shifts and broadening of the $Co2$ absorption line which affects the cross sections at measured wavelengths. The LBLRTM software incorporates these effects and computes a

175 numerical line shape function in OD at the given altitude of each layer. For the airborne data retrievals, meteorological data are obtained from the near real-time forward processing of the Goddard Modelling and Assimilation Office (GMAO) FP

system, the Goddard Earth Observing System Model, Version 5 (GEOS-5) (Rienecker et al., 2008). The data are drawn from the 8 per day analyzed fields on the full model grid (0.25 x 0.3125 degrees x 72 layers, inst3_3d_asm_Nv files). The GEOS-5 data are used for the meteorological conditions for the retrievals at the times and places where the airborne in situ profile measurements are not available. For analysis of our airborne campaign measurements the GEOS-5 data were used primarily except during the spiral maneuvers. We extract the nearest-in-time, latitude-longitude interpolated meteorological soundings from the GEOS-5 data every minute at regular positions along the flight's ground tracks. The 42 lowest analysis levels are used for each profile location. The analyzed pressure is used for the vertical grid coordinate for any of the profiles. The surface pressure and surface height are horizontally interpolated from the model.

Since the power and size of the CO_2 Sounder lidar are limited, there is a limit to the number of laser wavelengths which can be used to sample the XCO_2 absorption line at a given rate and maintain adequate SNR at each wavelength. Although Ramanathan et al. (2018) showed a few additional parameters about the CO_2 absorption line shape may be retrieved, they provide only limited information about the vertical profile of CO_2 mixing ratio. Therefore, we choose to retrieve a single scale factor for a reference profile, similar to the profile-scaling used in passive remote sensing (Borsdorff et al. 2014). Here the reference profile is obtained from the radiative transfer model and meteorological data described above. A least squares method is used to solve for the scale factor that minimizes the error between the line shape model and the lidar sampled CO_2 absorption line shape at all laser wavelengths. This retrieval method assumes that the modelled line shape is accurate. In practice, there may be differences between the model and the actual line shape which could cause biases in the solutions. However, if the modelling error is random, the approach of using lidar's sampling of the line at multiple wavelengths and using a line fit tends to average out the effect of the discrepancies.

Using the scale factor, the OD which is attributable to the CO_2 absorption can be written as

$$OD_{CO2}(\lambda_i) \approx \alpha_{CO2} \sum_{j=1}^{N2} xco2_a(H_j) \rho_{air}(H_j) \sigma_{CO2}(H_j, \lambda_i) \Delta H_j = \alpha_{CO2} OD_{CO2a}(\lambda_i) \tag{8}$$

where α_{CO2} is the scale factor, $xco2_a(H_j)$ is the *a priori* (initial guess) CO_2 mixing ratio at altitude H_j, and $OD_{CO2a}(\lambda_i)$ is the a priori total column OD attributed to CO_2 absorption. The atmospheric transmission due to CO_2 absorption can now be approximated as

$$T_{CO2}^2(\lambda_i) \approx exp\{-2 \alpha_{CO2} OD_{CO2a}(\lambda_i)\}. \tag{9}$$

4. Solving for XCO₂ from the Lidar Measurements via a Least-Squares Fit

The column XCO_2 and several other variables are solved simultaneously from a least-squares fit of the modelled line shape to the lidar measurements. One variable is the Doppler shift in the wavelengths of the received signal, which occurs when measuring at non-nadir angles from a moving platform. Another parameter being solved for is the product of the surface reflectance and the two-way off-line atmospheric transmission. For the CO_2 line at 1572.33 nm and under high humidity, there is a weak water vapor absorption feature on the left wing of the CO_2 absorption line. The retrieval algorithm can resolve this absorption feature to avoid causing biases in the retrieved XCO_2. For our airborne lidar, there is also small linear trend (slope)

in the received laser pulse energy as a function of the wavelength. The primary cause of this trend is the residual errors from modelling the uneven spectral response of the receiver optics, especially the optical bandpass filter. Since the bandpass spectral shape can change slightly with temperature and time, the retrieval also solves for this residual slope.

The least-squares fit may be formulated by expressing the lidar measurement data in matrix form, $\mathbf{Y}$, a single column matrix with elements y_i given by Eq. (2). The parameters to be solved for, $\mathbf{S} = \{s_k\}$, is expressed as a $N_3 \times 1$ matrix. In our case $N_3 = 5$, where each element is defined as

$s_1 = r_s T_o^2$ is the product of the surface reflectance and the two-way atmosphere transmission at off-line wavelength;

$s_2 = \alpha_{CO2}$ is the scale factor for the XCO$_2$ line shape function;

$s_3 = \alpha_{water}$ is the scale factor for the water vapor line shape function;

s_4 is the linear slope of the receiver spectral response; and

s_5 is the Doppler shift of the received signal wavelengths.

The modeled atmospheric transmission given in Eq. (9) can be expressed as a single column matrix, $\mathbf{F(S)}$, called forward model, with each element equal to

$$f_i(\mathbf{S}) = r_s T_A^2(\lambda_i, \mathbf{S}) \approx s_1 [s_2 T_{co2}^2(\lambda_i + s_5)][s_3 T_{water}^2(\lambda_i + s_5)]\eta_0(\lambda_i + s_5, s_4) \tag{10}$$

where $T_A^2(\lambda, \mathbf{S})$ is the atmosphere transmission defined in Eq. (1) but expressed as a function of both the laser wavelength and the parameters to be solved, and $\eta_0(\lambda, s_4)$ is the normalized receiver optical transmission as a function of the wavelength and the slope of the linear trend of the receiver spectral response. Here we also included the term for the water vapor.

A scalar-valued loss function can be defined as the sum of squared differences between the lidar measurement data and the model, as,

$$J(\mathbf{Y}, \mathbf{S}) = [\mathbf{Y} - \mathbf{F(S)}]^T \mathbf{W} [\mathbf{Y} - \mathbf{F(S)}] = \sum_{i=1}^{N_1} w_{i,i} [y(\lambda_i) - f_i(\mathbf{S})]^2 \tag{11}$$

where $[\mathbf{Y} - \mathbf{F(S)}]$ is an $N_1 \times 1$ matrix and $\mathbf{W}$ is a $N_1 \times N_1$ diagonal matrix for weighting factors used in the fit. The weighting factors are chosen to balance the contributions from the measurements at different laser wavelengths that have different SNRs. The least-squares fit finds the parameter set that minimizes the loss function.

For small changes in XCO$_2$ and for high SNR lidar measurements, Eq. (11) can be linearized by the first two terms of its power series expansion about initial estimates of the parameter values, $\mathbf{S0}$. The function $\mathbf{F(S)}$, also known as the forward model, can then be approximated by

$$\mathbf{F(S)} \approx \mathbf{F0} + \frac{\partial \mathbf{F(S)}}{\partial \mathbf{S}}\Big|_{\mathbf{S=S0}}(\mathbf{S} - \mathbf{S0}) \tag{12}$$

where

$$\mathbf{F0} = \mathbf{F(S0)} = \begin{bmatrix} f0(\lambda_1) \\ \vdots \\ f0(\lambda_{N_1}) \end{bmatrix}$$

with $f0(\lambda_i)$ equal to Eq. (10) evaluated at the initial value of the parameter set.

Substituting Eq. (12) into Eq. (11) and defining $\Delta \mathbf{Y} = (\mathbf{Y} - \mathbf{F0})$ and $\Delta \mathbf{S} = \mathbf{S} - \mathbf{S0}$, the loss function can now be

240 approximated as

$$J(\mathbf{Y}, \mathbf{S}) \approx \left[\Delta \mathbf{Y} - \frac{\partial \mathbf{F(S)}}{\partial \mathbf{S}}|_{\mathbf{S=S0}} \Delta \mathbf{S}\right]^{\mathrm{T}} \mathbf{W} \left[\Delta \mathbf{Y} - \frac{\partial \mathbf{F(S)}}{\partial \mathbf{S}}|_{\mathbf{S=S0}} \Delta \mathbf{S}\right]. \tag{13}$$

For mathematical convenience, we normalize the lidar measurements with respective to their initial estimate and define a new variable

$$\Delta y1(\lambda_{i1}) = \frac{\Delta y(\lambda_i)}{f0(\lambda_i)}. \tag{14}$$

245 A diagonal matrix $\mathbf{I_0}$ can be defined with each element equal to $1/f0(\lambda_i)$. The loss function can be rewritten using the identity matrix $\mathbf{I} \equiv \mathbf{I_0} \, \mathbf{I_0}^{-1} \equiv \mathbf{I_0}^{-1}\mathbf{I_0}$, as,

$$J(\mathbf{Y}, \mathbf{S}) \approx \left[\Delta \mathbf{Y} - \frac{\partial \mathbf{F(S)}}{\partial \mathbf{S}}|_{\mathbf{S=S0}}\Delta \mathbf{S}\right]^{\mathrm{T}} (\mathbf{I_0} \, \mathbf{I_0}^{-1})\mathbf{W}(\, \mathbf{I_0}^{-1}\mathbf{I_0}) \left[\Delta \mathbf{Y} - \frac{\partial \mathbf{F(S)}}{\partial \mathbf{S}}|_{\mathbf{S=S0}}\Delta \mathbf{S}\right]$$

$$= \left[\Delta \mathbf{Y1} - \frac{\partial \mathbf{F1(S)}}{\partial \mathbf{S}} \Delta \mathbf{S}\right]^{\mathrm{T}} \mathbf{W1} \left[\Delta \mathbf{Y1} - \frac{\partial \mathbf{F1(S)}}{\partial \mathbf{S}} \Delta \mathbf{S}\right] \tag{15}$$

where $\Delta \mathbf{Y1} = \mathbf{I_0}\Delta \mathbf{Y}$, $\mathbf{F1(S)} = \mathbf{I_0}\mathbf{F(S)}$, and $\mathbf{W1} = \mathbf{I_0}^{-1}\mathbf{W}\mathbf{I_0}$.

250 The use of the above normalization greatly simplifies the mathematical derivation as well as the data processing since it cancels out the exponential terms in $\mathbf{F(S)}$. However, this technique can only be used when the values of the forward model $f0(\lambda_i)$ are not approaching zero at all sampling wavelengths.

The loss function given in Eq. (13) is of the same form as that of a linear least-squares fit with measurement data $\Delta Y1$ and weighting factor $\mathbf{W1}$. The derivative of the function $\mathbf{F(S)}$, which is often referred to as the Jacobian, is given by

255 $\mathbf{K} = \frac{\partial [\mathbf{F1(S)}]}{\partial \mathbf{S}}|_{\mathbf{S=S0}}.$ $\tag{16}$

For the CO2 Sounder lidar, each term of the Jacobian can be derived as

$k_{i,1} = \frac{\partial F(S)}{s_1} \frac{1}{f0(\lambda_i)} = \frac{1}{\langle r_s T_o^2 \rangle}$, same for all $i = 1,2, \dots N_1$;

$k_{i,2} = -2\overline{OD}_{CO2}(\lambda_i)$, one for each laser wavelength, $i = 1,2, \dots N_1$;

$k_{i,3}$, same as above but for water vapor;

260 $k_{i,4} \approx \frac{T_{CO2}^2(\lambda_i+\Delta\lambda)-T_{CO2}^2(\lambda_i)}{\Delta\lambda} \cdot \frac{1}{\langle T_{CO2}^2(\lambda_i)\rangle}$, with $\Delta\lambda = 1 \, pm$ and $T_{CO2}^2(\lambda_i)$ given by Eq. (4); and

$k_{i,5} = (\lambda_i - \lambda_c)$, with λ_c the center wavelength of the CO2 line shape function.

For measurement noise that is zero-mean and follows a Gaussian distribution, the optimal weighting factors are given by the reciprocal of the variance of the measurement data (Bevington 1969). In our case, the optimal weighting factors can be approximated as

265 $w1_{i,i} = \frac{1}{var\{\Delta y1(\lambda_i)\}} = \frac{f0(\lambda_i)^2}{var\{y(\lambda_i)\}} \approx \frac{\langle y(\lambda_i)\rangle^2}{var\{y(\lambda_i)\}} = SNR(\lambda_i)^2$ $\tag{17}$

where $\langle y(\lambda_i)\rangle$ is the average value of the lidar measurement which is assumed to be close to the initial estimate $f0(\lambda_i)$. Therefore, for each wavelength the weighting factors can be approximated by the SNR of the lidar measurement at that

wavelength. As mentioned earlier, the SNRs are calculated based on signal energy and background noise estimated from received pulse waveforms.

270   The XCO2 and other parameters can now be solved using a standard linear least-squares fitting method with the loss function Eq. (15), Jacobian Eq. (16), and weighting factors Eq. (17). The solutions can be obtained numerically using the pseudo inverse function, as

$$\Delta\hat{S} = G\,\Delta Y1 \tag{18}$$

with G a $N_3 \times N_1$ matrix, which is often called gain matrix and can be computed from the pseudo inverse function $pinv(\cdot)$

275 (Peters and Wilkinson, 1970), as

$$G = pinv[K^T pinv(W1)K]\,K^T pinv(W1). \tag{19}$$

The pseudo inverse matrix function can be found in Matlab software package and in other software tools.

        The covariance of the parameters can be obtained from Eq. (18), as

$$cov(\Delta\hat{S}) = G^T\,var(\Delta Y1)\,G. \tag{20}$$

280 with $var(\Delta Y1)$ a diagonal matrix with the elements given by Eq. (17). The covariance matrix $cov(\Delta\hat{S})$ is in general not a diagonal matrix even though $var(\Delta Y1)$ is a diagonal matrix.

        The variances of the estimated parameters are given by the diagonal elements of $cov(\Delta\hat{S})$. However, variance is only one of the criteria of the XCO2 retrieval. There can still be a bias in the estimated parameters if there is a mismatch between the measurements and the modelled line shape.

285   The total column averaging kernel can be calculated as (Borsdorff et al., 2014),

$$A = G_\alpha K_x, \tag{21}$$

where G_α is the row of the G matrix for calculating the XCO2 scale factor and K_x is the Jacobian of the measurement with respective to the layered CO2 mixing ratios, which is an $N_1 \times N_2$ matrix given by

$$K_x = \frac{\partial F(xco2)}{\partial xco2}. \tag{22}$$

290 Each term of K_x can be written according to Eqs. (2)-(4), (7), and (10), as

$$K_x(i,j) = \rho_{air}(H_j)\,\sigma_{CO2}(H_j, \lambda_i)\,\Delta H_j.$$

        The linear least-squares fit can also be iterated by correcting for the Doppler shift of the received laser wavelengths of the modeled line shape based on the solution from the previous iteration. The Jacobian terms are recalculated about the updated linearization point in each iteration to improve the results.

295 **5. Evaluation of the Retrieval Algorithm Using Airborne Lidar Data**

The algorithm described here was used to retrieve XCO2 from measurements of our 2017 airborne lidar campaign (Mao et al., 2019). The lidar and the airborne measurements have been described in detail in Abshire et al. (2018). Table 1 lists the instrument parameters relevant to the XCO2 retrieval. Here we show a few examples of using the retrieval algorithm on a data

set collected during one of the 2017 flights. We also show the retrieved XCO_2 at different altitudes in comparison to XCO_2

300 calculated from the in situ measurements made during two spiral-down maneuvers.

Table 1. The airborne CO_2 Sounder lidar instrument parameters.

Instrument Parameters	Values
Laser:	
Pulse energy	25 μJ
Wavelength scan range	1572.235-1572.440 nm
Number of wavelengths	30 (see Fig. 5)
Wavelength accuracy	0.008 pm (1 MHz)
Spectral line width	< 0.247 pm (30 MHz)
Pulse width	1 μs
Pulse rate	10 kHz
Divergence angle	0.43 mrad (4.3 m laser spot size on ground from a 10 km altitude)
Receiver Optics	
Telescope size	20 cm diameter
Field of view	0.50 mrad
Optical filter bandwidth	1.4 nm
Total optical transmission	81.3%
Detector and Receiver Electronics	
Quantum efficiency, including fill factor	69%
Responsivity	6.39×10^8 V/W
Noise equivalent power (NEP), 16 pixels combined	6.9 fW/Hz$^{1/2}$
Signal sample rate	100 MHz, 16 bits
Integration time for each XCO_2 retrieval	1 sec
Data recording duty cycle	90%

Figure 4 shows an example of a Level-1data set from our 2017 airborne campaign. It shows 30 transmitted pulse

305 waveforms and the corresponding received pulse waveforms averaged over 32 laser wavelength scans. The decrease (tilt) of

laser pulse amplitudes over the pulse width interval is caused by the depletion of energy stored in the laser gain media, which

does not affect the IPDA lidar measurements. The energies of the transmitted laser pulses at different wavelengths fluctuate

by a few percent, which is monitored and corrected for in the signal processing. The tails in the transmitted pulse waveforms

shown in Fig. 4 (b) are caused by an artifact of the laser monitor detector, which is different from the one used in the receiver.

310 The amplitudes and energies of the received laser pulse waveform plotted in Fig. 4 (c) clearly show the CO_2 absorption near

the center of the wavelength scan. The XCO_2 retrieval is carried out at 1 Hz, during which the host aircraft typically travels

about 200 m.
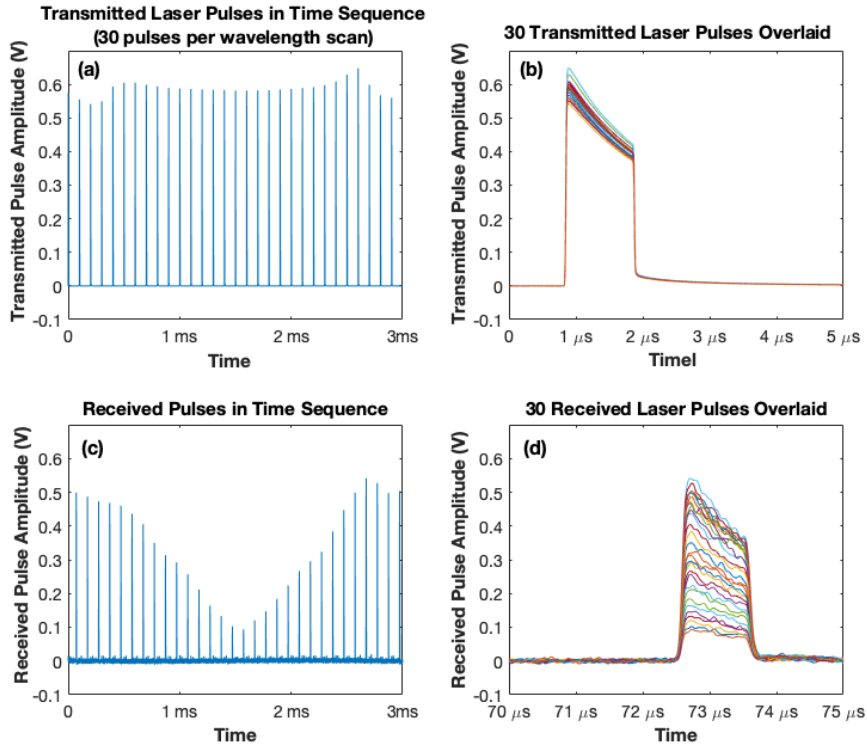
Figure 4. Sample pulse waveforms of the airborne CO_2 Sounder lidar taken during the flight of 7/21/2017 00:30:00 (UTC) (local time 7/20/2017 17:30:00). (a) The 30 transmitted laser pulse waveforms in a wavelength scan averaged over 32 repeated scans; (b) overlay of transmitted pulse waveforms (c) the corresponding received laser pulse waveforms reflected from the ground surface showing the lidar sampled CO_2 absorption, and (d) an overlay of the received pulse waveforms for all 30 laser wavelengths.

For the least-squares fit the weighting factor for each wavelength is the square of the SNR of the lidar detected signals at that wavelength. The SNRs are estimated from the received lidar signal as (Gagliardi and Karp, 1995)

$$SNR(\lambda_i) = \frac{\eta_d \langle n_s(\lambda_i) \rangle}{\sqrt{F_d \left[\eta_d \left(n_s(\lambda_i) + \left(1 + \frac{\tau_s}{\tau_b} \right) \langle n_b \rangle \right) + \left(1 + \frac{\tau_s}{\tau_b} \right) \langle n_d \rangle \right] + \left(1 + \frac{\tau_s}{\tau_b} \right) \langle n_a \rangle^2 / \langle G_d \rangle^2}} . \tag{25}$$

Here $\langle n_s(\lambda_i) \rangle$ is the average number of received signal photons per pulse at wavelength λ_i, $\langle G_d \rangle$ is the average gain of the avalanche photodiode (APD) detector, η_d is the APD quantum efficiency, F_d is the APD gain excess noise factor, τ_s is the integration time for the signal pulse, τ_b is the integration time for the background and dark noise, $\langle n_b \rangle$ and $\langle n_d \rangle$ are the average number of background photons and detector dark counts integrated over the pulse interval, and $\langle n_a \rangle$ is the standard deviation of the preamplifier noise in terms of equivalent number of photoelectrons. The signal here refers to the number of detected

signal photons, which is equal to the difference of the number of the detected photons minus the number of detected background

330   photons.

The laser speckle noise term (Goodman 1965, 1975) is not included in Eq. (25), since it is not a major noise source for our airborne lidar measurements at nominal flight altitude. This is because of the large number of speckle cells in the laser footprint and the numerical averaging of the 30 received laser pulses for each XCO_2 retrieval. Laser speckle noise is also not expected to be a major noise source for the space version of the CO_2 Sounder lidar being developed at NASA GSFC (see

335   chapter 5 of Kawa et al., 2018) since the effects of spatial and numerical averaging are similar. The effects of errors in the meteorological data used to construct the line shape model of CO_2 is also not considered in Eq. (25). We are currently conducting computer simulations to quantify the effect of meteorological data errors and the results will be reported in a separate publication.

For the XCO_2 retrieval, the average number of received signal photons is estimated from the received pulse waveform.

340   This is obtained by first integrating the received pulse waveform from the detector in volts, dividing the result by the detector responsivity in volts/watt, and the photon energy in Joules. The average number of background noise photons is estimated from the average surface reflectance, off-line atmosphere transmission, the nominal sun light irradiance on the surface, and the receiver optics model. All other parameter values in Eq. (24) are instrument related and can be found in Abshire et al. (2018).

345   Figure 5 shows the CO_2 absorption line shape sampled by the lidar along with that from the forward model which assumes a constant XCO_2 vertical profile of 400 parts per million (ppm). It also shows the placement of laser wavelengths across the CO_2 absorption line. One laser wavelength (the second from the left) was placed at a secondary absorption feature due to deuterated water vapor (HDO). Three wavelengths were placed on the wings of the CO_2 absorption line. The rest were roughly equally spaced in OD along the absorption line. The residual differences between the measurements and the model after the

350   least-squares fit is also plotted in Fig. 5. The averaging kernel is calculated based on Eq. (22) for each fit of 1-second lidar measurement data. Figure 6 shows the normalized averaging kernel with respected to its average value over the atmosphere column height and a fourth order polynomial fit for the data shown above.

Figure 7 shows the results of the retrieval using the algorithm described above from the airborne CO_2 Sounder lidar measurements made on 21 July 2017 starting at 00:30:00 for 820 seconds. The data consist of about a 500 second segment

355   measured at a nearly constant aircraft altitude followed by about 300 seconds of measurements in a spiral descent. The last part of the flight was near Edwards Air Force Base, CA and the surface elevation was nearly constant for the last 500 seconds. The ground surface over this stretch of the flight was dry desert and the sky was visually clear at the time. The retrieved XCO_2 over this period was steady with a slow downward trend. The root-mean-squared (rms) variation of the retrieved XCO_2 from 2100 to 2300 seconds was 0.67 ppm, which includes both the fitting error and the actual XCO_2 variation along the flight path.

360   By comparison, the estimated standard deviation from the retrieval covariance matrix was about 0.35 ppm, as shown in Fig. 7(e).
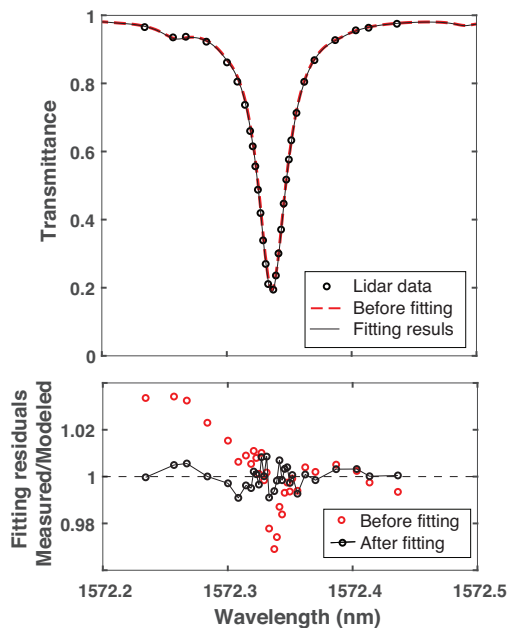
Figure 5. Top, an example of a CO_2 absorption line shape sampled by the airborne lidar (black circles) for 1-sec averaging time and the models before and after the fit (red and black lines). Bottom, differences (the residuals) between the lidar measurement and the models at the lidar wavelengths before (in red circles) and after (in black circles) the least-squares fit for the data set shown in Fig. 4. The retrieved scale factor was $\alpha_{xco2} \approx 1.025$ (i.e. 410 ppm retrieved vs. 400 pm assumed).
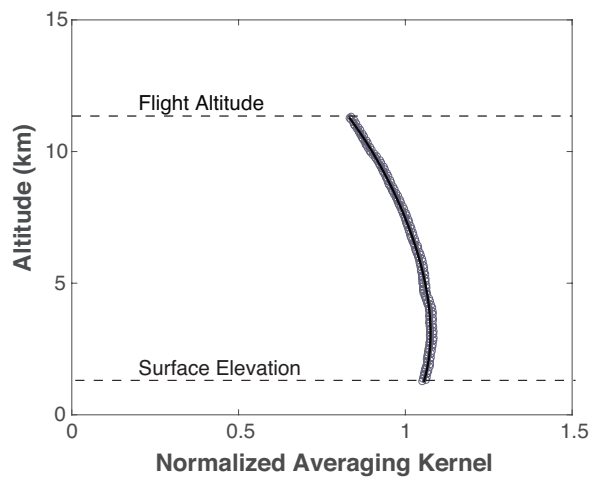
Figure 6. The averaging kernel from the retrieved data (open circles) and the 4th order polynomial fit with altitude (solid black curve) from the measurement data shown in Fig. 5.
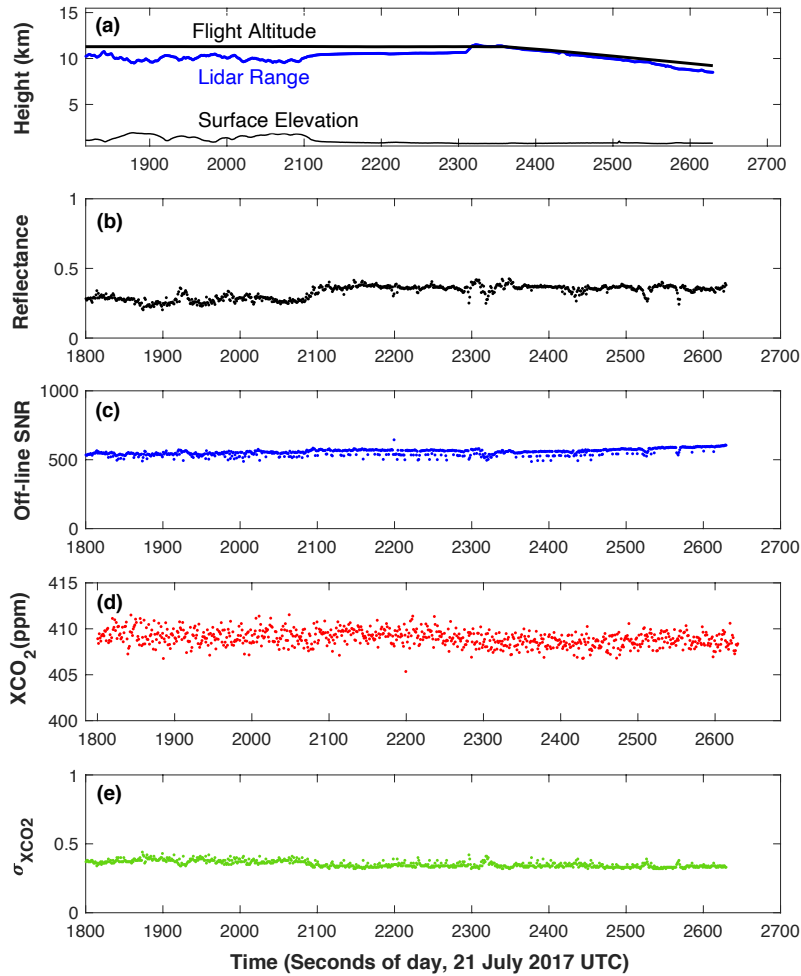
Figure 7. The results of the retrieval sequence from the airborne CO_2 Sounder lidar data starting at 21 July 2020 00:30:00 UTC for 820 seconds over Edwards Air Force Base in California. These are all based on 1-second receiver integration time. They are, from top down, (a) the aircraft altitude, the lidar range from the laser pulse time of flight, and surface elevation computed from the on-board GPS receiver, the lidar range and pointing angles (b) the retrieved surface reflectance times the two-way off-line atmospheric transmission; (c) off-line SNR calculated from Eq. (24); (d) the retrieved XCO_2; and (e) standard deviation of the retrieved XCO_2 from the covariance matrix. The airplane velocity was about 200 m/s. The distance covered by the data shown in the plot is about 164 km.

Figure 8 shows the retrieved XCO$_2$ compared to that calculated from in situ measurements as the airplane flew in a spiral-down path from 12 km to 4 km over Edwards Air Force Base for the flight on July 21, 2017 and for that on August 8, 2017. The in situ profiles were measured by an updated version of the AVOCET gas analyzer on board the airplane (Vay et al., 2011). The in situ XCO$_2$ is calculated from the airplane altitude to the ground and is obtained by integrating the CO$_2$ profile from the in situ measurements weighted by the lidar's averaging kernel. The XCO$_2$ retrieved from the lidar measurements agrees with that calculated from the in situ measurements at all airplane altitudes above 4 km. Below 4 km, the laser beam no longer completely overlaps the field of view of the receiver and the total CO$_2$ absorption (line depth) becomes small. The lidar measurements are not calibrated at such low altitude.
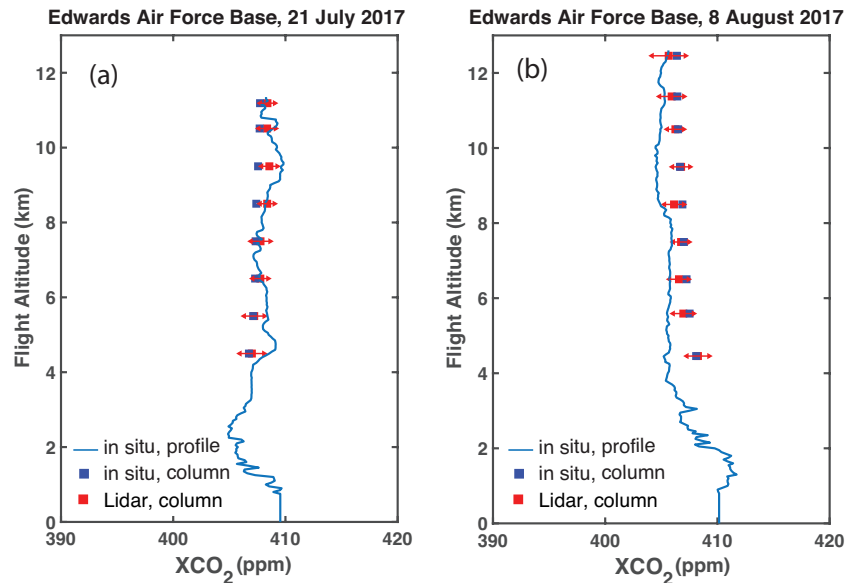
Figure 8. The column XCO$_2$ from the aircraft to the surface retrieved from the lidar measurements (red squares) compared to that computed from the in situ measurements (blue squares) during the spiral-downs on (a) 21 July 2017, near the end of the data segment shown in Fig. 7 and (b) 8 August 2017. The error bars on the red squares represent mean and the standard deviation of the lidar measurement results binned into 1-km layers. The blue squares are the column mixing ratio integrated from the readings of the AVOCET gas analyzer from the flight altitude to the surface. For the spiral-down comparisons, the median differences (biases) between the retrieved lidar and column in situ measurements are 0.72 ppm for 21 July and 0.16 ppm for 8 August 2017.

6. Discussion

6.1 Biases in the Retrieved XCO2

Although the least-squares-fit method minimizes the sum of squared errors between the modelled line shape and the lidar measurements, it does not guarantee minimum biases in the estimated parameters. The variance of the solutions can approach zero as the SNR increases, as shown in Eq. (18), but bias remains. For example, if the actual CO_2 absorption line shape does not match that of the model, the retrieved results can be biased regardless of the SNR. Therefore, it is important to model the atmosphere and the absorption spectroscopy accurately and avoid systematic errors.

6.2. Choice of Laser Wavelengths

The choice of the lidar laser wavelengths is a trade-off among several factors. The total number of laser wavelengths has to be greater than the number of parameters to be solved for in the retrieval, however, the total average laser output power is fixed. Using fewer wavelength samples allows improving the SNR for each sample, but provides fewer constraint to the curve fit. More wavelength samples lowers the SNR at each wavelength, but allows solving for more parameters and helps to reduce the bias in the XCO_2 retrieval. There is also an advantage to select the laser wavelengths to be symmetrically distributed about the line center since it reduces the effect of the nonuniformity in the receiver's spectral response (Chen et al., 2019). Finally, the laser wavelengths should not be placed where the CO_2 absorption is too high, e.g., OD>1.5, since the received signal level becomes too low to contribute to the retrieval.

The airborne CO_2 Sounder lidar mostly used 30 wavelengths with four off-line, four near the center of the peak absorption up to OD=1.2, one on the water vapor peak absorption, and the rest approximately uniformly distributed in OD (Abshire et al, 2018). This choice of the laser wavelengths produced measurement precisions < 1 ppm and biases < 1 ppm. Abshire et al., (2018) also report airborne measurement made using 15 laser wavelengths that showed no apparent difference in the XCO_2 measurements to those using 30 wavelengths for the otherwise same instrument configuration.

The retrieval algorithm described in this paper could also be used for the on- and off-line dual wavelength IPDA lidar to retrieve XCO_2 and the product of surface reflectance and two-way atmosphere transmission. The solution to the least squares fit for the two parameters can be derived analytically and becomes the same as those reported earlier (Abshire et al., 2010). The standard deviation of the retrieved XCO_2 at a given average laser power can be lower compared to that of a multi-wavelength IPDA lidar, depending on the placement of the on-line wavelength. However, the Doppler shift, water vapor content, and the receiver spectral response would have to be obtained and corrected well enough to avoid XCO_2 bias. The results would be much more sensitive to uncertainties in the CO_2 absorption line shape.

6.3. Number of Parameters to Retrieve

It is possible to use the least-squares fit to solve for more parameters of the CO_2 line and lidar instrument, as long as the information content of the lidar measurements support them. However, solving for more parameters, especially when they are

correlated, increases the variance in the retrieved values, which limits the benefit. One example is to divide the atmosphere into a few layers, each with its own line shape function and scale factor, to obtain some information about the vertical distribution of XCO_2. The results from the least-squares fit for the XCO_2 for the layers, however, are correlated and the errors from the fits are usually too large to be useful (Chen et al., 2014). A singular value decomposition (SVD) method also has been used to extract a few more parameters about the line shape without the need for an a priori vertical XCO_2 profile (Ramanathan et al., 2018). For measurement with high SNR, the SVD method can retrieve some characteristics of the line shape, such as the line width, and provide some constraints about the vertical distribution of XCO_2

Conclusion

An algorithm to retrieve XCO_2 has been developed for measurements from a pulsed multi-wavelength IPDA lidar. The retrieval algorithm uses a least-squares fit of the line shape function derived from a multi-layer atmosphere radiative transfer model based on meteorological data to the line shape sampled by the lidar measurements. In addition to XCO_2, the algorithm simultaneously solves for the product of the surface reflectance and the off-line atmosphere transmission, Doppler shift of the received laser signals, a secondary water vapor mixing ratio (if present), and a linear trend of the lidar receiver non-uniformity in its spectral response. Since it can accurately retrieve XCO2 as these conditions vary, this approach provides a more robust measurement of XCO_2 compared to IPDA lidar that use only on-line and off-line wavelengths. The retrieval algorithm has been used successfully in the data processing of the NASA Goddard multi-wavelength pulsed IPDA lidar from its 2016 and 2017 airborne campaigns. The algorithm may also be used for retrievals for multi-wavelength lidars that target other atmospheric gases, such as CH_4.

Acknowledgements. The CO_2 Sounder lidar development was supported by the NASA ESTO Instrument Incubator program and the flights were supported by the NASA ASCENDS Mission preformulation program. We thank the CO_2 Sounder lidar team at NASA Goddard for the development of the lidar, conducting the airborne campaigns, and collecting the measurement data. We also thank Joshua P. Digangi for the AVOCET measurements, Julie Nicely for updating and testing the software for the XCO_2 retrieval, and Jeffrey Chen for many technical discussions about XCO_2 retrievals.

References

Abshire, J. B., Riris, H., Allan, G. R., Weaver, C., Mao, J., Sun, X., Hasselbrack, W. E., Kawa, S. R., and Biraud, S.: Pulsed airborne lidar measurements of atmospheric CO2 column absorption, Tellus B, 62(5), 770-783, https://doi.org/10.1111/j.1600-0889.2010.00502.x, 2010.

Abshire, J. B., Riris, H., Weaver, C., Mao, J., Allan, G., Hasselbrack, W., and Browell, E. V.: Airborne measurements of
460   CO_2 column absorption and range using a pulsed direct-detection integrated path differential absorption lidar, Appl.
       Optics, 52, 4446–4461, https://doi.org/10.1364/AO.52.004446, 2013.

Abshire, J. B., Ramanathan, A., Riris, H., Mao, J., Allan, G. R., Hasselbrack, W. E., Weaver, C. J., and Browell, E.V.:
       Airborne measurements of CO_2 column concentration and range using a pulsed direct-detection IPDA lidar, Remote
       Sens., 6, 443–469, https://doi.org/10.3390/rs6010443, 2014.

465   Abshire, J. B., Ramanathan, A., Riris, H., Allan, G. R., Sun, X., Hasselbrack, W. E., Mao, J., Wu, S., Chen, J., Numata, K.,
       Kawa, S. R., Ying, M., Yang, M., and DiGangi, J.: Airborne measurements of CO_2 column concentrations made with a
       pulsed IPDA lidar using multiple-wavelength-locked laser and HgCdTe APD detector, Atmos. Meas. Tech., 11, 2001-
       2025, https://doi.org/10.5194/amt-11-2001-2018, 2018.

Amediek, A., Ehret, G., Fix, A., Wirth, M., Büdenbender, C., Quatrevalet, M., Kiemle, C., and Gerbig, C.: CHARM-F: A
470   new airborne integrated-path differential-absorption lidar for carbon dioxide and methane observations: measurement
       performance and quantification of strong point source emissions, Appl. Optics, 56, 5182–5197,
       https://doi.org/10.1364/AO.56.005182, 2017.

Allan, G. R., Sun, X., Abshire, J. B., Riris, H., Hasslbrack, W. E., Kawa, S. R. Numata, K., Mao, J. and Chen, J.: Atmospheric
       backscattering profiles from the 2017 ASCENDS/ABoVE airborne campaign measured by the CO_2 Sounder lidar, 2019
475   Fall AGU Annual Meeting, San Francisco, CA, Dec. 9-13, 2019, Paper A51M-2726.

Bevington, P. R.: Data Reduction and Error Analysis for the Physical Science, McGraw-Hill, New York, 1969, Ch. 6.

Campbell, J. F., Lin, B., Dobler, J., Pal, S., Davis, K., Obland, M. D., Erxleben, W., McGregor, D., O'Dell, C., Bell, E., Weir,
       B., Fan, T-.F., Kooi, S., Gordon, I., Corbett, A., Kochanov, R.: Field evaluation of column CO_2 retrievals from intensity-
       modulated continuous-wave differential absorption lidar measurements during the ACT-America campaign, Earth Space
480   Sci., 7, e2019EA000847, https://doi.org/10.1029/2019EA000847, 2020.

Borsdorff, T., Hasekamp, O. P., Wassmann, A., Landgraf, J.: Insights into Tikhonov regularization: application to trace gas
       column retrieval and the efficient calculation of total column averaging kernels, Atmos. Meas. Tech., 7, 523-535,
       https://doi.org/10.5194/amt-7-523-2014, 2014.

Chen, J. R., Numaa, K., and Wu, S. t.: Error reduction methods for integrated-path differential-absorption lidar measurements,
485   Opt. Express, 20, 15590-15609, https://doi.org/10.1364/OE.20.015589, 2012.

Chen, J. R., Numata, K., and Wu, S. T.: Error reduction in retrieval of atmospheric species from symmetrically measured lidar
       sounding absorption spectra, Opt. Express, 22, 26055-26075, https://doi.org/10.1364/OE.22.026055, 2014.

Chen, J. R., Numata, K., and We, S. T.: Impact of broadened laser line-shape on retrieval of atmospheric species from lidar
       sounding absorption spectra, Opt. Express, 23, 2660-2675, https://doi.org/10.1364/OE.23.002660, 2015.

490   Chen, J. R., Numata, K., and Wu, S. T.: Error analysis for lidar retrievals of atmospheric species from absorption spectra, Opt.
       Express, 27, 36487-36504, https://doi.org/10.1364/OE.27.036487, 2019.

Clough, S. A., Iacono, M. J. and Moncet, J.: Line-by-line calculations of atmospheric fluxes and cooling rates: Application to water vapor, J. Geophys. Res. Atmos. 97, 15,761-715,785, https://doi.org/10.1029/92JD01419, 1992.

Clough, S. A. & Iacono, M. J.: Line-by-line calculation of atmospheric fluxes and cooling rates 2. Application to carbon dioxide, methane, nitrous oxide and the halocarbons, J. Geophys. Res. Atmos. 100, 16,519-516,535, https://doi.org/10.1029/95JD01386, 1995.

Crisp, D., Pollock, H. R., Rosenberg, R., Chapsky, L., Lee, R. A. M., Oyafuso, F. A., Frankenberg, C., O'Dell, C. W., Bruegge, C. J., Doran, G. B., Eldering, A., Fisher, B. M., Fu, D., Gunson, M R., Mandrake, L., Osterman, G. B., Schwandner, F. M., Sun, K., Taylor, T. E., Wennberg, P. O., and Wunch, D.: The on-orbit performance of the Orbiting Carbon Observatory-2 (OCO-2) instrument and its radiometrically calibrated products, Atmos. Meas. Tech. 10, 59-81, https://doi.org/10.5194/amt-10-59-2017, 2017.

Dobler, J., Harrison, F., Browell, E., Lin, B., McGregor, D., Kooi, S., Choi, Y., and Ismail, S.: Atmospheric CO2 column measurements with an airborne intensity-modulated continuous wave 1.57 um fiber laser lidar, Appl. Optics, 52, 2874–2892, https://doi.org/10.1364/AO.52.002874, 2013.

Eldering, A., O'Dell, C. W., Wennberg, P., Crisp, O. D., Gunson, M. R., Viatte, C., et al.: The Orbiting Carbon Observatory-2: first 18 months of science data products, Atmos. Meas. Tech., 10, 549–563, https://doi.org/10.5194/amt-10-549-2017, 2017.

Eldering, A., Taylor, T. E., O'Dell, C. W., and Pavlick, R.: The OCO-3 mission: measurement objectives and expected performance based on 1 year of simulated data, Atmos. Meas. Tech., 12, 2341–2370, https://doi.org/10.5194/amt-12-2341-2019, 2019.

Gagliardi, R. M. and Karp, S.: Optical Communications, 2nd ed, John Wiley and Sons, 1995.

Goodman, J. W.: Some effects of target-induced scintillation on optical radar performance, Proc. IEEE, 55, 1688-1700, https://doi.org/10.1109/PROC.1965.4341, 1965.

Goodman, J. W.: Statistics properties of laser speckle patterns, in Laser Speckle and Related Phenomena, Dainty, J. C. ed., Spinger-Verlag, Berlin Heidelberg, 9-75, 1975.

Han, G., Shi, T., Ma, X., Xu, H., Zhang, M., Liu, Q., and Gong, Wei, G.: Obtaining gradients of XCO2 in atmosphere using the constrained linear least-squares technique and multi-wavelength IPDA LiDAR, Remote Sens., 12, 2395, https://doi.org/10.3390/rs12152395, 2020.

Jacob, J. C., Menzies, R. T., and Spiers, G. D.: Data processing and analysis approach to retrieve carbon dioxide weighted-column mixing ratio and 2-μm reflectance with an airborne laser absorption spectrometer, IEEE Trans. Geosci. Remote Sens., 57(2), 958-971, https://doi.org/10.1109/TGRS.2018.2863711, 2019.

Kawa, S. R., Abshire, J. B., Sun, X., Mao, J., and Ramanathan, A.: Updated performance simulations for a space-based CO2 lidar mission, 12th International Workshop on Greenhouse Gas Measurements from Space (IWGGMS-12), Jun. 7-9, 2016, Kyoto, Japan, Paper 48, https://www.nies.go.jp/soc/events/iwggms12/pdf/Session_10/48_Stephan_Kawa.pdf.

525   Kawa, S. R., Abshire, J. B., Baker, D. F., Browell, E. V., Crisp, D., Crowell, S. M. R., Hyon, J. J., Jacob, J. C., Jucks, K. W.,
      Lin, B., et al.: Active Sensing of CO2 Emissions over Nights, Days, and Seasons (ASCENDS): Final Report of the
      ASCENDS, Ad Hoc Science Definition Team, Document ID: 20190000855, NASA/TP–2018-219034, GSFC-E-DAA-
      TN64573, 2018, https://www-air.larc.nasa.gov/missions/ascends/docs/NASA_TP_2018-219034_ASCENDS_ID1.pdf.

      Kuze, A., Suto, H., Shiomi, K., Kawakami, S., Tanaka, M., Ueda, Y., Deguchi, A., Yoshida, J., Yamamato, Y., Kataoka, F.,
530   Taylor, T. E., and Buijs, H. L., Update on GOSAT TANSO-FTS performance, operations, and data products after more
         than 6 years in space, Atmos. Meas. Tech., 9, 2445–2461, https://doi.org/10.5194/amt-9-2445-2016, 2016.

      Mao, J., Ramanathan, A., Abshire, J. B., Kawa, S. R., Riris, H., Allan, G. R., Hasselbrack, W. E., Sun, X., Chen, J., and
         Numata, K.: Atmospheric CO_2 concentration measurements to cloud tops from airborne lidar measurement during
         ASCENDS science campaigns, Atmos. Meas. Tech., 11, 127-140, https://doi.org/10.5194/amt-11-127-2018, 2018.

535   Mao, J., Abshire, J. B., Kawa, S. R., Riris, H., Allan, G. R., Hasselbrack, W. E., Numata, K., Chen, J., Sun, X., Nicely, J. M.,
         DiGangi, P. J., and Choi, Y.: Airborne demonstration of atmospheric cO2 concentration measurements with a pulsed
         multi-wavelength IPDA lidar, 15th International Workshop on Greenhouse Gas Measurements from Space (IWGGMS),
         Jun. 3-5, 2019, Sapporo, Japan, Paper 5-5, www.nies.go.jp/soc/doc/Oral_Presentations/Session5-6/5-
         5_iw15op_Jianping_Mao.pdf.

540   Menzies, R. T., Spiers, G. D., and Jacob, J.: Airborne laser absorption spectrometer measurements of atmospheric CO_2
         column mole fractions: source and sink detection and environmental impacts on retrievals, J. Atmos. Ocean Technol.,
         31, 404-421, https://doi.org/10.1175/JTECH-D-13-00128.1, 2014.

      McManamon, P.: LiDAR, Technologies and Systems, SPIE Press, Bellingham, 2019, Ch. 3.

      Peters, G. and Wilkinson, J. H.: The least squares problem and pseudo-Inverses, The Computer Journal, 13, 309-316,
545   https://doi.org/10.1093/comjnl/13.3.309, 1970.

      Numata, K., Chen, J. R., and Wu, S. T.: Precision and fast wavelength tuning of a dynamically phase-locked widely-tunable
         laser, Opt. Express, 20, 14234-14243, https://doi.org/10.1364/OE.20.014234, 2012.

      Ramanathan, A., Mao, J., Allan, G. R., Riris, H., Weaver, C. J., Hasselbrack, W. E., Browell, E. V., and Abshire, J. B.:
         Spectroscopic measurements of a CO2 absorption line in an open vertical path using an airborne lidar, Appl. Phys. Lett.,
550   103, 214102, https://doi.org/10.1063/1.4832616, 2013.

      Ramanathan, A. K., Mao, J., Abshire, J., and Allan, G. R.: Remote sensing measurements of the CO_2 mixing ratio in the
         planetary boundary layer using cloud slicing with airborne lidar, Geophys. Res. Lett., 42, 2055-2062,
         https://doi.org/10.1002/2014GL062749, 2015.

      Ramanathan, A. K., Nguyen, H. M., Sun, X., Mao, J., Abshire, J. B., Hobbs, J. M., and Braverman, A. J.: A singular value
555   decomposition framework for bias-free retrievals with vertical distribution information from column greenhouse gas
         absorption spectroscopy measurements, Atmos. Meas. Tech., 11, 4909-4928, https://doi.org/10.5194/amt-11-4909-2018,
         2018.

      Refaat, T. F., Singh, U. N., Yu, J., Petros, M., and Ismail, S.: Double-pulse 2-μm integrated path differential absorption lidar

airborne validation for atmospheric carbon dioxide measurement, Appl. Optics, 55, 4232-4246, https://doi.org/10.1364/AO.55.004232, 2016.

Refaat, T. F., Petros M., Singh, U. N., Antill, C. W., and Remus, Jr., R. G.: High-precision and high-accuracy column dry-air mixing ratio measurement of carbon dioxide using pulsed 2-μm IPDA lidar, IEEE Trans. Geosci. Remote Sens., 58(8), 5804-5819, https://doi.org/10.1109/TGRS.2020.2970686, 2020.

Refaat, T. F., Petros, M., Antill, C. W., Singh, U. N., Choi, Y., Plant, J. V., Digangi, J. P., and Noe, A.: Airborne testing of 2-μm pulsed IPDA lidar for active remote sensing of atmospheric carbon dioxide, Atmosphere, 12, 412, https://doi.org/10.3390/atmos12030412, 2021.

Rienecker, M. M., Suarez, M.J., Gelaro, R.; Todling, R., Bacmeister, J., Liu, E.; Bosilovich, M.G., Shubert, S.D., Takacs, L., Kim, G.-K., et al.: MERRA: NASA's modern-era retrospective analysis for research and applications, J. Clim., 24, 3624–3648, https://doi.org/10.1175/JCLI-D-11-00015.1, 2011.

Rodgers, C. D.: Inverse Methods for Atmospheric Sounding, *Theory and Practice*, World of Scientific Publishing, Singapore, 2000.

Rothman, L., et al.: The HITRAN 2008 molecular spectroscopic database, J. Quant. Spectros. Radiat. Transfer, 110(9), 533–572, https://doi.org/10.1016/j.jqsrt.2009.02.013, 2009.

Sellers, P. J., Schimel, D. S., Moore III, B., Liu, J., and Eldering, A.: Observing carbon cycle–climate feedbacks from space, Proceedings of the National Academy of Science of the United States of America, 115, 7860–7868, https://doi.org/10.1073/pnas.1716613115, 2018.

Spiers, G., Menzies, R., Jacob, J., Christensen, L., Phillips, M., Choi, Y., and Browell, E.: Atmospheric CO2 measurements with a 2 μm airborne laser absorption spectrometer employing coherent detection, Appl. Optics, 50, 2098–2111, https://doi.org/10.1364/AO.50.002098, 2011.

Vay, S. A., Choi, Y., Vadrevu, K. P., Blake, D. R., Tyler, S. C., W., Woo, J.-H., Weinheimer, A. J., Burkhart, J. F., Stohl, A., and Wennberg, P. O., Wisthaler, A., Hecobian, A., Kondo, Y., Diskin, G. S., and Sachse, G.: Patterns of CO2 and radiocarbon across high northern latitudes during International Polar Year 2008, J. Geophys. Res.-Atmos., 116, D14301, https://doi.org/10.1029/2011JD015643, 2011.

Zhu, Y., Liu, J., Chen, X., Zhu, D. B., and Chen, W.: Sensitivity analysis and correction algorithms for atmospheric CO_2 measurements with 1.57-μm airborne double-pulse IPDA LIDAR, Opt. Express, 27, 32679-32699, https://doi.org/10.1364/OE.27.032679, 2019.

Zhu, Y., Yang, J., Chen, X., Zhu, X., Zhang, J., Li, S., Sun, Y., Hou, X., Bi, D., Bu, L., Zhang, Y., Liu, J., and Chen, W.: Airborne validation experiment of 1.57-μm double-pulse IPDA lidar for atmospheric carbon dioxide measurement, Remote Sens., 12, 1999, https://doi.org/10.3390/rs12121999, 2020.